WATER RESOURCES RESEARCH, VOL. 36, NO. 3, PAGES 781–785, MARCH 2000

Infiltration with controlled air escape

Patricia J. Culligan,[1] D. A. Barry,[2] J.-Yves Parlange,[3] Tammo S. Steenhuis,[3] and Randel Haverkamp[4]

Abstract. Infiltration into the soil is restricted if the movement of displaced air is hampered. In this study, separate infiltration experiments were performed where the air could escape only through capillary glass tubes (three different diameters were used). Control experiments, where the air movement was not restricted, were performed also. During the experiments both air pressure and the cumulative infiltration were measured. Air pressure measurements showed a rapid rise to a maximum after the water was ponded, followed by a gradual decrease. A first aim of this study was to show that even for a small increase in pressure relative to the case where the air was free to escape, e.g., <1 cm of water, there was a small but measurable reduction in infiltration. The air movement was obtained as a function of the air pressure via Poiseuille's law. By equating air and water movement (both fluids assumed incompressible) it was shown that the air pressure measurements could be used in predicting the water flux into the column and hence the cumulative infiltration. Then, by using the precise air pressure measurements for the various capillary tubes we were able to assess the sensitivity of hydraulic conductivity and sorptivity to minor increases in air pressure.

1. Introduction

The infiltration rate in a soil can be reduced significantly if there is resistance to air movement, and it can be accompanied by air entrapment and air bubbling through the soil surface. This has been well documented in the field [*Dixon and Linden*, 1972; *Starr et al*., 1978] and in the laboratory [*Brooks and Corey*, 1966; *MacWhorter*, 1971; *Vachaud et al*., 1974; *Touma et al*., 1984; *Wang et al*., 1997]. Theory and numerical studies relating to the movement of air and water have also been presented [*Youngs and Peck*, 1964; *Sander and Parlange*, 1984; *Sander et al*., 1988a, b, c; *Weir and Kissling*, 1992].

We analyze column infiltration experiments in which we control the air flow so that the air pressure cannot reach a level such that the soil structure is affected. Additionally, we measure the air pressure during the infiltration process and deduce from those measurements the water flux into the soil column. The maximum pressure allowed will be the natural bubbling pressure at the beginning of infiltration when the continuity of air paths is preserved. By controlling the pressure we also consider cases when the pressure is much less than the bubbling pressure, i.e., when there is little resistance to air flow, but even in that case we could observe a significant decrease in infiltration. Finally, we could estimate the soil properties and investigate the sensitivity of those properties to minor changes in the measured air pressures.

[1]Department of Civil and Environmental Engineering, Massachusetts Institute of Technology, Cambridge.
[2]School of Civil and Environmental Engineering, University of Edinburgh, Edinburgh, Scotland.
[3]Department of Agricultural and Biological Engineering, Cornell University, Ithaca, New York.
[4]Centre National de la Recherche Scientifiques, LTHE/IMG, UJF, INPG, URA 1512, Grenoble, France.

Paper number 1999WR900351.
0043-1397/00/1999WR900351$09.00

2. Theory

Consider one-dimensional flow in a soil column with a uniform initial moisture content θ_i. The column is sealed except for a capillary tube located with one end within the soil and the other open to the atmosphere. The experiment begins when water is ponded to a fixed depth at the surface. We use a general infiltration equation that is valid for any size capillary whether or not it is small enough for the air to reach the bubbling pressure [*Haverkamp et al*., 1990]

$$I^* = \frac{\gamma}{q^* - 1} + (1 - \gamma) \ln \frac{q^*}{q^* - 1}, \tag{1}$$

where I is the cumulative infiltration, q is the flux, and γ is a constant. The definitions of the dimensionless variables (indicated by asterisks) are

$$I^* = I \frac{2K_s}{S^2 + 2K_s h_{\text{surf}}(\theta_s - \theta_i)} \tag{2}$$

$$t^* = t \frac{2K_s^2}{S^2 + 2K_s h_{\text{surf}}(\theta_s - \theta_i)} \tag{3}$$

$$q^* = dI^*/dt^*, \tag{4}$$

where t is time, K_s is the natural saturated conductivity, S is the sorptivity, i.e., $I = S\sqrt{t}$ when $t \to 0$ and $h_{\text{surf}} = 0$ and when $h_{\text{surf}} \neq 0$, the influence of the latter is given explicitly by the denominator, e.g., of (2), h_{surf} is the pressure head at the surface, and $(\theta_s - \theta_i)$ is the difference between the saturated and the (assumed uniform) initial water contents. Finally,

$$\gamma = \frac{2K_s(h_{\text{surf}} - h_{str})(\theta_s - \theta_i)}{S^2 + 2K_s h_{\text{surf}}(\theta_s - \theta_i)}. \tag{5}$$

Previously, use of this model was based on the assumption that the air pressure in the soil remains atmospheric [*Haverkamp et al*., 1988]. In our experiments, where the air escapes through a glass capillary tube, the air pressure head ahead of the infiltrating front (assumed spatially uniform), h_a,

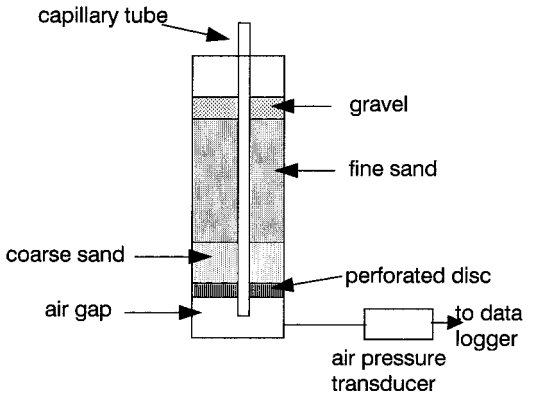

Figure 1. Schematic diagram of the experimental setup.

is positive. Denoting the thickness of the ponded layer of water at the soil surface by h_p, the pressure head driving the flow through the surface of the soil is then given at all times by

$$h_{\text{surf}} = h_p - h_a, \tag{6}$$

which decreases as expected when the air pressure head is atmospheric ($h_a = 0$), in which case the surface matric potential is equal to the depth of ponded water.

By definition, $h_{str} < 0$ is equal to the initial straight part of the soil moisture characteristic curve near saturation. Also, $|h_{str}|$ is usually small but has a noticeable influence on infiltration [*Barry et al*., 1995]. If some minor bubbling takes place through the soil surface during a very short time immediately after infiltration begins, at this time the air pressure in the soil h_a is by definition the bubbling pressure h_b. Then, $(h_p - h_b)$ is the matric potential at the surface during that short period when the larger pores just desaturate, i.e., $h_{\text{surf}} = h_{st}$. Thus

$$h_{str} = h_p - h_b \tag{7}$$

As bubbling lasts a very short time, alternate methods like that of *Fallow and Elrick* [1996] could not be used. Thus (7) is a convenient way to estimate it, when h_b is measured accurately, as it is in the experiments reported below. Note that with bubbling, $h_{\text{surf}} = h_{str} < 0$, but the results of *Haverkamp et al*. [1988] still apply as long as h_{surf} is in the vertical (straight) part of the water retention curve, i.e., $h_{\text{surf}} \geq h_{str}$ and bubbling corresponds to the smallest value of h_{surf} when the results can be applied.

We now rewrite (1)–(4) when dimensionless variables are expressed using h_p rather than h_{surf} since h_p rather than h_{surf} is imposed. These variables are indicated by a superscript o. Thus I^o and t^o are the values of I^* and t^* when h_{surf} in (2) and (3) is replaced by h_p. Note that because the denominators are the same in (2) and (3), $q^o = dI^o/dt^o = q^*$. With this notation, (1) yields

$$I^o = \frac{\gamma_o(1 - h_a/h_b)}{q^o - 1} + (1 - \gamma_o) \ln \frac{q^o}{q^o - 1}, \tag{8}$$

where the constant γ^o is the value of γ when h_{surf} is replaced by h_p. The advantage of (8), which predicts the cumulative infiltration for a known soil when $h_a(t)$ is measured, is that it shows clearly the reduction in cumulative infiltration due to increase in air pressure. After bubbling has stopped, or from the beginning of the experiment when there is no bubbling, air escapes through a glass capillary tube of known diameter d and length L. Treating air as incompressible (it can be easily shown that the variation in the volume of air due to the measured increase of air pressure is a secondary effect which has a small but observable effect as discussed later) and the air flow as laminar, Poiseuille's law applies, i.e.,

$$q^o K_s = \frac{\pi d^4 \rho_w g h_a}{128 \mu_a L A}, \tag{9}$$

where A is the cross-sectional area of the column, ρ_w is the density of water, and μ_a is the viscosity of air. Under these conditions we obtain two remarkable results: First, because measurement of h_a is relatively easy, (9) provides an estimate of the flux directly without necessitating the differentiation of I, which is more difficult given the normal scatter of experimental data. Second, eliminating h_a in (8) with (9) yields a differential equation for I^o, or

$$I^o = \gamma_o \frac{(1 - \varepsilon q^o)}{q^o - 1} + (1 - \gamma_o) \ln \left(\frac{q^o}{q^o - 1} \right), \tag{10}$$

where ε is a constant given by

$$\varepsilon = 128 A K_s \mu_a l / \pi d^4 \rho_w g h_b. \tag{11}$$

3. Materials and Methods

Experiments were performed in a 50-cm-high Perspex column having an internal diameter of 11.4 cm. An evenly perforated Perspex disc (1/2-cm thick) supported on three pillars was used to form a 5-cm-high air gap at the base of the column. Above this was placed 500 g of uniform coarse sand, having an average particle diameter of ~0.1 cm. This was overlain by ~30 cm of fine sand uniformly packed to an average density of 1.66 ± 0.01 g cm^{-3}. Above the fine sand, 500 cm^3 of gravel drainage material was added to prevent surface erosion. In all experiments with capillary tubes, a 55.5-cm-long glass capillary tube, having an internal diameter (ID) of either 3.14×10^{-2}, 2.53×10^{-2}, or 1.58×10^{-2} cm, was introduced at the center of the column throughout the full height of soil. The porosity of the soil in each experiment θ_s was calculated directly using knowledge of the particle density. For our experiments we packed the fine sand in the column, so that $\theta_s = 0.375$, with little variation.

A schematic diagram of the experimental setup is given in Figure 1. A 160PC 1-psi (6895 Pa) signal conditioned pressure transducer, manufactured by Micro Switch and having a sensitivity of 5V/psi, was used to measure the air pressure at the base of the column. During each experiment, signals from the transducer were recorded at 0.1-s intervals using the laboratory data-logging system.

Each experiment followed the same general procedure. First, the soil column was packed dry. Next, a fixed level of water 3.2 cm above the fine sand layer was introduced. The cumulative infiltration was obtained directly by measuring the amount of water to maintain the water level at 3.2 cm. Both cumulative infiltration and the air pressure were then recorded for the duration of the experiment. The experiment was continued until the wetting front reached the underside of the column and visual observation indicated that the wetting front reached that underside uniformly in all experiments; that is, there were no "cracks" in the packing, especially along the walls or the capillary, and no fingering could develop in the short coarse sand layer. Of course, the theory was used only as

long as the wetting front was observed in the fine sand layer. The experiment for each capillary tube size and without capillary when air is free to move out at the bottom of the column was replicated six times.

4. Results and Discussion

Figure 2 shows typical measurements of air pressure with narrow, medium, and large capillary tubes. We note some erratic variations, which are more apparent for the top curve (narrow tube) and could be easily removed by filtering high frequencies. However, as we shall see later, it is useful to keep them as a measure of the uncertainty of the present experimental procedure. The reason for using the narrow capillary is to provide a direct measurement of h_{str}, as mentioned earlier. We see that in all cases the pressure increases rapidly to a maximum in a few seconds. When no bubbling occurs, the maximum is very sharp, whereas the maximum is flat as bubbling takes place. This maximum gives, easily and simply, an estimate of h_b for our fine sand

$$h_b \approx 5.8 \pm 0.2 \text{ cm}. \tag{12}$$

The uncertainty of ± 0.2 cm is surprisingly small given that the chamber was repacked for each replicate experiment (six in total, as mentioned above). We shall see later that infiltration is insensitive to those small variations. The value of h_p being 3.2 cm, (1) yields,

$$h_{str} = -2.6 \pm 0.2 \text{ cm}. \tag{13}$$

In the case of the medium capillary, middle curve in Figure 2, the pressure drops rapidly to $<1/2$ and $<1/4$ cm for the large capillary, the bottom curve in Figure 2. These background pressures have only a small effect on infiltration: We can calculate, using (8), that after 150 s, the reduction in cumulative infiltration is ~ 1 cm for the medium and 1/2 cm for the large capillary tube, when compared to the case when $h_a = 0$, i.e., when there is no resistance to air escape and the air remains at atmospheric pressure. Figure 3 shows direct measurement of I as a function of time with the medium capillary (only the two experiments out of six showing the highest and lowest I are shown to give an idea of the maximum error due to repacking

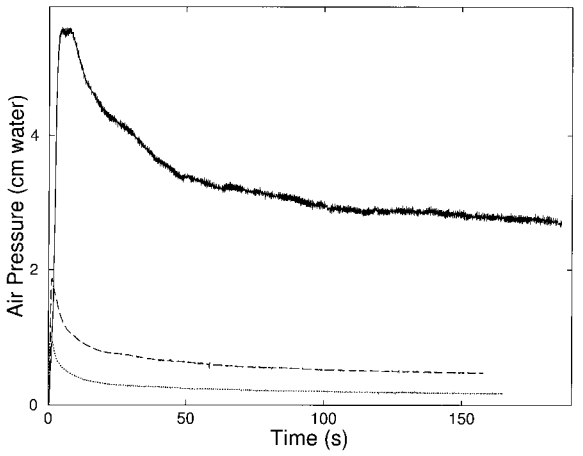

Figure 2. Air pressure with time: from top to bottom, capillary tube with 0.158-, 0.253-, and 0.314-mm internal diameter (ID).

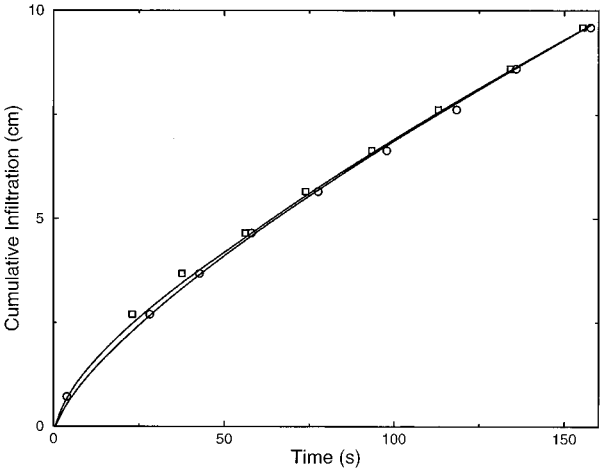

Figure 3. Measured (squares and circles) and calculated with (14) (solid lines) cumulative infiltration for the two extremes of six experiments with the medium capillary tube, 0.253-mm ID.

the column). More importantly, Figure 3 also shows the cumulative infiltration deduced by integrating (9) with time, i.e.,

$$I = \frac{\pi d^4 \rho_w g}{128 \mu_a L A} \int_0^t h_a(\bar{t})\, d\bar{t}. \tag{14}$$

The traces obtained by integrating the measured air pressure h_a (corresponding to lowest and highest measured I) show excellent agreement with the observed data. Thus (9) is, indeed, a reliable equation, and hence the present procedure allows us to measure directly the flux from h_a without any need of differentiation. Note also that the variability in I obtained by the integration of h_a is less than by the direct measurement (Figure 2) as expected. For short times the continuous values of I tend to be a little bit lower than the observed values (although within the scatter of the data). This may be due to the slight effect of air compressibility at early times, which becomes very small as time progresses. In the following, when we refer to the flux q and cumulative infiltration I, we mean the values obtained from h_a via (9) and $\int h_a\, dt$ via (14), respectively. The interest of this procedure is to obtain essentially continuous, rather than discrete, values of I, as well as reliable values of q. Similar results are obtained with the large capillary. As compared with the medium tube, we observe that the underprediction due to air compressibility for the large tube in early times is even less noticeable than for the medium tube.

Figure 4 shows, again, the two extreme measurements when the air is free to move through the bottom of the column ($h_a = 0$). The dashed line and the three solid lines correspond to predictions with different soil water properties as discussed later. The pluses and diamonds are the experimental cumulative infiltration data for the extremes of the replicates. The dotted line shows the integrated air pressure data for the experiment corresponding to the diamonds. Clearly, this method of determining the cumulative infiltration remains very accurate in all cases.

The saturated conductivity K_s was measured independently (from flux measurements in a saturated column) and was found to be 0.0375 ± 0.0015 cm s^{-1}, the variability being due to the small variations in packing density [*Parlange et al.*, 1988] between experiments and inhomogeneities in the column.

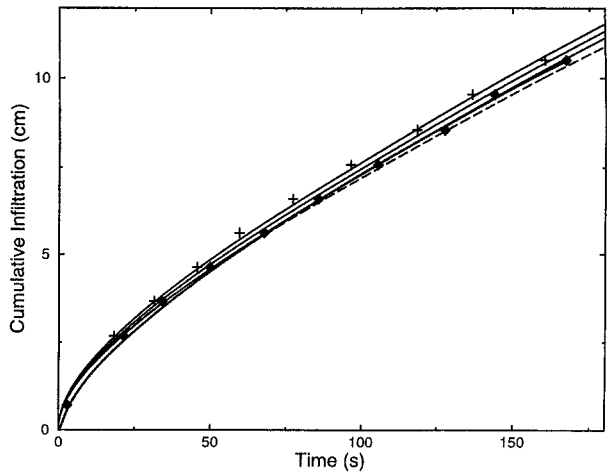

Figure 4. Infiltration with no air flow restriction. The pluses and diamonds are data showing the range due to experiment replication. The three solid lines correspond to $K_s = 0.0375$ cm s^{-1}, $h_{str} = 2.6$ cm, and $S = 0.41$ cm s$^{-1/2} \pm 0.03$. The dashed line is the predicted infiltration for the same K_s and $S = 0.41$ cm s$^{-1/2}$ but $h_{str} = 0$. The dotted line (lowest curve at the origin) is the prediction determined using (14) for the experiment represented by the diamonds.

However, the present method also gives us the means to calculate K_s and its variation in time during infiltration, i.e., the method reveals the influence of inhomogeneities, as discussed below.

Comparing the change in I between two experiments at different times but when the fluxes are equal, then (10) gives (reverting back to dimensional quantities)

$$\Delta I = -(h_p - h_{str})(\theta_s - \theta_i)\left(\frac{q}{q - K_s}\right)\Delta\varepsilon, \qquad (15)$$

where $\Delta\varepsilon$, from (11), is due to the change in the factor d^4 between experiments. Figure 5 shows ΔI versus the flux q (where both are obtained from pressure measurements). The two experiments used to calculate ΔI are from the top and bottom cases of Figure 2, i.e., the small and large capillaries (to enhance the value of $\Delta\varepsilon$). The three lines correspond to K_s (in cm s^{-1}) = 0.0365, 0.0375, and 0.0385, respectively. The results are consistent with the independent measurements of K_s. It is quite interesting that the high-frequency fluctuations of the pressure gage (or associated electronics) show as a jagged line in Figure 5. The fluctuations are due primarily to the small diameter capillary (see Figure 2) and are more pronounced for the lower fluxes and are a useful measure of the uncertainty of the experimental procedure. However, overall, we find that the overall variability of K_s between experiments is similar to the variability of K_s within experiments.

The value of the sorptivity S can now be determined. Note that with the present method, S and K_s are obtained separately; that is, we do not have to curve fit infiltration data to obtain the two parameters simultaneously. We now illustrate the method to obtain S. Figure 6 gives q versus I for the two extreme cases of Figure 3 from (10) (for the large capillary). Note again the increasing influence of the high-frequency behavior at lower fluxes and also that the variability between experiments is comparable to that within an experiment. The three solid lines correspond to $K_s = 0.0375$ cm s^{-1} and to $S = 0.41$ cm s$^{-1/2} \pm 0.03$ (i.e., $S = 0.38$, 0.41, and 0.44 cm s$^{-1/2}$), which captures most of the overall variability in the data. A very slightly different way to use the same data is to plot S, from (10), with $K_s = 0.0375$ cm s^{-1}, as a function of I directly. Doing so, we found that again, $S = 0.41$ cm s$^{-1/2} \pm 0.03$ captures most of the variability (for I small the values of S tend to decrease slightly, most likely due to the small compressibility effect).

Having obtained values of h_{str}, S, and K_s, we now return to the important practical case of predicting infiltration when air is free to escape. Observe that from the analysis presented above we have all the soil parameters needed to predict infiltration, i.e., no curve/parameter fitting is needed. The three solid lines in Figure 4 correspond to $K_s = 0.0375$ cm s^{-1}, $h_{str} = 2.6$ cm, and $S = 0.41$ cm s$^{-1/2} \pm 0.03$. Those three curves capture most of the variability in the data. Not to overly clutter Figure 4, we did not plot the effect of the ± 0.015 cm s^{-1} measured variation in K_s, which only increases the spread of

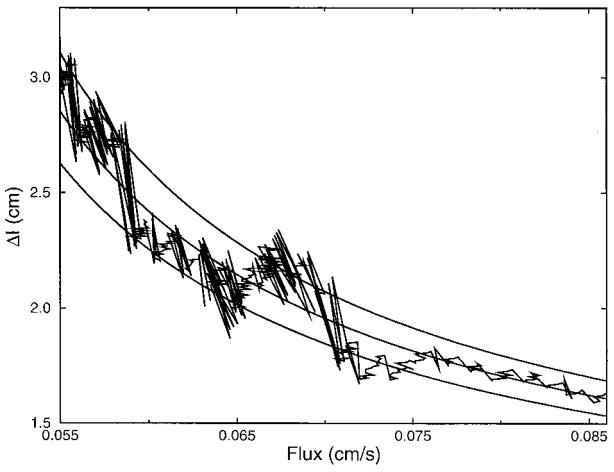

Figure 5. Plot of ΔI versus flux for data from two experiments with capillary tube of 0.158- and 0.314-mm ID. The three solid smooth lines are calculated with (15) with K_s of 0.0365, 0.0375, and 0.0385 cm s^{-1}. The jagged line is obtained using (9) and (14) and the top and bottom curves in Figure 2.

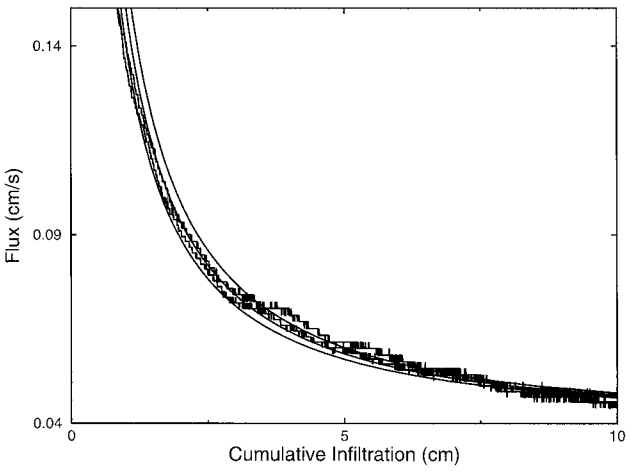

Figure 6. Plot of flux q versus cumulative infiltration I. The smooth solid lines are obtained from (10) with $K_s = 0.0375$ cm s^{-1} and $S = 0.38$, 0.41, and 0.44 cm s$^{-1/2}$, respectively. The jagged solid line is obtained, as in Figure 5, with the bottom curve in Figure 2.

the curves a little. The lower, dashed line is for $S = 0.41$ cm $s^{-1/2}$ but for $h_{str} = 0$. The effect on infiltration is small, of the order of the scatter in the data, which confirms that the uncertainty on h_{str}, ± 0.2 cm, is irrelevant.

Finally, note that an interesting consequence of air escaping through a capillary tube is that $q(t \to 0)$ is finite. Equation (10) shows at once that for ε small,

$$q_o(t \to 0) \approx (\varepsilon \gamma_o)^{-1} - \tfrac{1}{2}(1 - \gamma_o) + O(\varepsilon \gamma_o), \qquad (16)$$

thus avoiding the usual (mathematical) difficulty of an infinite flux as $t \to 0$. However, it is doubtful that (16) is of practical interest as the measured flux/pressure at very short times is influenced by air compressibility. This is shown in Figure 4 where, as $t \to 0$, the dotted line, representing the integration of the pressure data (affected by compressibility), is slightly different from the solid lines (which ignore it).

5. Conclusion

The case just discussed, i.e., predicting infiltration based on the properties, illustrates the difficulties in curve fitting $I(t)$ when the soil parameters are not known or are only crudely estimated. If, for instance, we had assumed, a priori, that $h_{str} = 0$, then we could fit the data by erroneously increasing S. In particular, by taking $S = 0.47$ cm $s^{-1/2}$ the dashed line would practically go on top of the middle solid line, thus curve fitting properties with limited experiments may be accurate but can easily lead to incorrect values of soil properties and could lead to poor prediction when used for conditions different from those of the measurements. Because of the extreme accuracy in measuring h_a we were able to analyze each parameter, S, K_s and h_{str}, independently.

We found that small air pressure ahead of the wetting front, i.e., $h_a \sim 1/4$ cm, had near-negligible effect on infiltration, yet the pressure measurement is used to calculate the flux and the cumulative infiltration by integration (which is far more accurate than measuring by differentiation of cumulative infiltration data). Another advantage of our measurements is that we obtained h_{str} directly from bubbling experiments and have confirmed [*Haverkamp et al*., 1990] that this parameter has small but noticeable effect on infiltration.

References

Barry, D. A., J.-Y. Parlange, R. Haverkamp, and P. J. Ross, Infiltration under ponded conditions, 4, An explicit predictive infiltration formula, *Soil Sci*., *160*, 8–17, 1995.

Brooks, R. H., and A. T. Corey, Properties of porous media affecting fluid flow, *J. Irrig. Drain. Eng*., *IR2*, 61–88, 1966.

Dixon, R. M., and D. R. Linden, Soil air pressure and water infiltration under border irrigation, *Soil Sci. Soc. Am. J*., *36*, 948–953, 1972.

Fallow, D. J., and D. E. Elrick, Field measurement of air-entry and water-entry soil water pressure heads, *Soil Sci. Soc. Am. J*., *60*, 1036–1039, 1996.

Haverkamp, R., M. Kutilek, J.-Y. Parlange, L. Rendon, and M. Krejca, Infiltration under ponded conditions, 2, Infiltration equations tested for parameter time-dependence and predictive use, *Soil Sci*., *145*, 317–329, 1988.

Haverkamp, R., J.-Y. Parlange, J. L. Starr, G. Schmitz, and C. Fuentes, Infiltration under ponded conditions, 3, A predictive equation based on physical parameters, *Soil Sci*., *149*, 292–300, 1990.

Jalalifarhani, H. R., H. R. Duke, and D. F. Heermann, Physics of surge irrigation, 1, Quantifying soil physical parameters, *Trans. ASAE*, *36*, 37–44, 1993.

MacWhorter, D. B., Infiltration affected by flow of air, *Hydrol. Pap. 49*, Colorado State Univ., Fort Collins, 1971.

Parlange, J.-Y., R. Haverkamp, C. W. Rose, and I. Phillips, Sorptivity and conductivity measurement, *Soil Sci*., *145*, 385–388, 1988.

Sander, G. C., and J.-Y. Parlange, Water and air movement in soils: An application of Brutsaert's and optimization techniques, *Soil Sci*., *138*, 198–202, 1984.

Sander, G. C., J.-Y. Parlange, and W. L. Hogarth, Extension of the Fujita solution to air and water movement in soils, *Water Resour. Res*., *24*, 1187–1191, 1988a.

Sander, G. C., J.-Y. Parlange, and W. L. Hogarth, Air and water flow, part 1, Horizontal flow with an arbitrary flux boundary condition, *J. Hydrol*., *99*, 215–223, 1988b.

Sander, G. C., J.-Y. Parlange, and W. L. Hogarth, Air and water flow, part 2, Gravitational flow with an arbitrary flux boundary condition, *J. Hydrol*., *99*, 225–234, 1988c.

Starr, J. L., H. C. de Roo, C. R. Fink, and J.-Y. Parlange, Leaching characteristics of a layered field soil, *Soil Sci. Soc. Am. J*., *42*, 386–391, 1978.

Touma, J., G. Vachaud, and J.-Y. Parlange, Air and water flow in a sealed, ponded vertical soil column: Experiment and model, *Soil Sci*., *137*, 181–187, 1984.

Vachaud, G., J. P. Gaudet, and V. Kuraz, Air and water flow during ponded infiltration in a bounded column of soil, *J. Hydrol*., *22*, 89–108, 1974.

Wang, Z., J. Feyen, D. R. Nielsen, and M. T. van Genuchten, Two-phase flow infiltration equations accounting for air entrapment, *Water Resour. Res*., *33*, 2759–2768, 1997.

Weir, G. J., and W. M. Kissling, The influence of air-flow on the vertical infiltration of water into soil, *Water Resour. Res*., *28*, 2765–2772, 1992.

Youngs, E. G., and A. J. Peck, Moisture profile development and air compression during water uptake by bounded porous bodies, 1, Theoretical introduction, *Soil Sci*., *98*, 290–294, 1964.

D. A. Barry, School of Civil and Environmental Engineering, University of Edinburgh, Edinburgh, Scotland, EH9 3JN, United Kingdom.

P. J. Culligan, Department of Civil and Environmental Engineering, Massachusetts Institute of Technology, Cambridge, MA 02139.

R. Haverkamp, LTHE/IMG, UJF, CNRS-URA 1512, P.O. Box 53X, 38041, Grenoble, France.

J.-Y. Parlange and T. S. Steenhuis, Department of Agricultural and Biological Engineering, Cornell University, Ithaca, NY 14853. (tss1@cornell.edu)

(Received October 6, 1999; revised December 6, 1999; accepted December 8, 1999.)